Chinese Journal of Aeronautics, (2023), 36(8): 43–53

Chinese Society of Aeronautics and Astronautics
& Beihang University

Chinese Journal of Aeronautics

cja@buaa.edu.cn
www.sciencedirect.com

Force measurement using strain-gauge balance in shock tunnel based on deep learning

Shaojun NIE [a,b], **Yunpeng WANG** [a,*], **Zonglin JIANG** [a,b]

[a] *State Key Laboratory of High Temperature Gas Dynamics, Institute of Mechanics, Chinese Academy of Sciences, Beijing 100190, China*
[b] *School of Engineering Science, University of Chinese Academy of Science, Beijing 100049, China*

Received 30 June 2022; revised 3 August 2022; accepted 22 September 2022
Available online 12 May 2023

KEYWORDS

Convolutional neural networks;
Deep learning;
Frequency domain analysis;
Force measurement;
Time domain analysis;
Recurrent neural networks

Abstract When a force test is conducted in a shock tunnel, vibration of the Force Measurement System (FMS) is excited under the strong flow impact, and it cannot be attenuated rapidly within the extremely short test duration of milliseconds order. The output signal of the force balance is coupled with the aerodynamic force and the inertial vibration. This interference can result in inaccurate force measurements, which can negatively impact the accuracy of the test results. To eliminate inertial vibration interference from the output signal, proposed here is a dynamic calibration modeling method for an FMS based on deep learning. The signal is processed using an intelligent Recurrent Neural Network (RNN) model in the time domain and an intelligent Convolutional Neural Network (CNN) model in the frequency domain. Results processed with the intelligent models show that the inertial vibration characteristics of the FMS can be identified efficiently and its main frequency is about 380 Hz. After processed by the intelligent models, the inertial vibration is mostly eliminated from the output signal. Also, the data processing results are subjected to error analysis. The relative error of each component is about 1%, which verifies that the modeling method based on deep learning has considerable engineering application value in data processing for pulse-type strain-gauge balances. Overall, the proposed dynamic calibration modeling method has the potential to improve the accuracy and reliability of force measurements in shock tunnel tests, which could have significant implications for the field of aerospace engineering.

1. Introduction

With rapid developments in the aerospace industry, research into hypersonic vehicles is now highly prevalent internationally. To reduce the risk and cost of developing a new hypersonic vehicle, it is necessary to conduct ground tests in a high-enthalpy shock tunnel to test its aerodynamic performance.[1–3] As one of the most basic and important techniques in shock-tunnel tests, force measurement is an important way to obtain the aerodynamic data of an aircraft, and its measurement accuracy will directly affect the evaluation of aerodynamic characteristics.[4]

Measuring accurately the aerodynamic forces acting on a hypersonic vehicle in a millisecond shock tunnel still involves many key technical problems, the main one being the inertial

* Corresponding author.
E-mail address: wangyunpeng@imech.ac.cn (Y. WANG).

https://doi.org/10.1016/j.cja.2023.05.009

vibration of the Force Measurement System (FMS), the main elements of which are the model, the wind-tunnel balance, and the supporting structure.[5–7] When a force test is carried out in a shock tunnel, disturbance of the complex flow field induces the inertial vibration with low frequency and high amplitude of the FMS, and the balance signal is mixed with the inertial vibration signals of the FMS, which makes it difficult to distinguish the dynamic characteristics of the aerodynamic signals directly and accurately. Therefore, it is very important to find a method for eliminating inertial vibration interference, provide reliable aerodynamic data, and develop highly accurate force measurement technology for developing hypersonic vehicles.

To eliminate inertial vibration interference from balance output signals, much research has been conducted and various special balance technologies have been proposed. Currently, there are three main methods for improving force measurement technology, the first involving the development of the new FMS. In some such approaches, the natural frequency of the FMS is enhanced by increasing its stiffness or improving its structure, thereby accelerating the attenuation of its inertial vibration and suppressing interference of the balance signal as much as possible; examples include the stress-wave balance, the piezoelectric balance, the magnetic suspension balance, the free flight technique, and the pulse-type strain-gauge balance. However, the stress-wave balance is greatly affected by unknown factors, so there is no assurance that the stress wave generated by the model can be transmitted effectively to the sensor of the balance.[8–12] Also, the stability of the piezoelectric balance based on piezoelectric ceramics is relatively poor and cannot satisfy actual test commands.[13] Li et al. designed the integrated force tests of balance and supporting structure by using magnetic suspension balance, which reduced the interference of flow field caused by FMS. [14,15] Furthermore, the accuracy of free flight technique is limited by the high-speed camera, and the technique is still developing.[16–19] Compared with the above technique, the pulse-type strain-gauge balance is more suitable for force tests in shock tunnel because of its improved dynamic performance, that is, higher accuracy and stronger stability.[20–22] Therefore, there is a bottleneck to eliminate the influence of inertial vibration through developing a new FMS.

The second method is to eliminate the influence of inertial vibration on the aerodynamic forces through signal compensation, examples being the accelerometer balance[23–26] and the inertial self-compensation balance.[27–29] However, when the frequency of the FMS vibration is close to that of the aerodynamic signal, it is difficult to identify the aerodynamic force accurately by self-compensation, which may lead to greater errors and thus incorrect results.

The third method involves balance signal processing. Luo et al. proposed a new signal decomposition method, wave system fitting, to remove vibration waves of low frequency. To reduce the systematic errors, they proposed a new calibration method, weighting by cross-validation, the effectiveness of which has been verified by force tests in a shock tunnel.[30,31] Nie and Wang used wavelet transform and Hilbert-Huang transform to process the balance signal and identified different interference signals, but this method is not suitable for processing low-frequency and short-duration signals.[32] Wang et al. applied deep learning to the FMS in an impulse facility and proposed a new dynamic calibration method known as Single-Vector Dynamic self-Calibration (SVDC). They used an intelligent Convolutional Neural Network (CNN) model to process the sample signal in the time domain, recognized the dynamic characteristics of the inertial vibration signal, and obtained relatively ideal aerodynamic results.[33] Wang et al. developed an intelligent identification algorithm for aerodynamics by combining time–frequency transform with deep learning, and finally obtained the real aerodynamic signal.[34].

In summary, it is very difficult to improve the measurement accuracy by either improving the balance structure or using signal compensation. Instead, the deep cross application of artificial-intelligence technology in force tests has become a trend that has considerable engineering significance.

The balance output signal in the time domain can offer an effective reflection of the force states of the FMS over time. A Recurrent Neural Network (RNN) is good at solving problems related to time sequences, so a RNN model can be used to process the balance output signal in the time domain for dynamic calibration. Also, inertial vibration and aerodynamic force differ considerably in the frequency domain: the frequency of inertial vibration is constant because it is an inherent attribute of the FMS, whereas the frequency of aerodynamic force varies with time.

Therefore, according to the different characteristics of the balance signal in the time and frequency domains, in this paper, we use different intelligent models and explore their differences, so as to improve the processing performance of balance data and the reliability of intelligent models. Fig. 1 shows the part system of the JF-12 hypersonic detonation-driven shock tunnel with long test duration (referred to herein as the JF-12 shock tunnel).[35] For the FMS of the JF-12 shock tunnel, a series of balance signal samples were collected, and their vibration characteristics were trained based on an RNN model in the time domain and a CNN model in the frequency domain. The trained intelligent models were then used to process the balance output signal in a force test, and a reliable quasi-steady aerodynamic signal was obtained.

2. Acquisition of balance signal samples

2.1. Early dynamic calibration study (SVDC)

To ensure accuracy in a force test, it is necessary to calibrate the balance before the test, including both static and dynamic calibration. Static calibration technology is now relatively mature, but there have been few studies of dynamic calibration to date.

Fig. 1 Photo of JF-12 shock tunnel.

The main traditional dynamic signal generation methods are impulse response[36,37] and step response.[38] Impulse response involves using an impact hammer to hit the model surface to generate an impulse force, but its direction and action point cannot be controlled accurately. Step response involves loading by hanging a weight in the fixed direction of the balance; after the FMS is stable, the weight is released immediately and a step unloading signal is generated. These traditional dynamic calibration methods have strict requirements for the load direction, so they cannot be used for the dynamic calibration of a shock-tunnel balance. To meet the requirement that the balance outputs multicomponent load signals in any direction, the SVDC technology was proposed. This method introduces deep-learning technology that can conduct modeling and processing for dynamic calibration in any direction and accurately identify the aerodynamic force coupled with inertial vibration interference.

The SVDC method generates a single vector in any direction of the balance via a steel wire connected to the FMS's suspension point. This single vector load can be decomposed automatically into multicomponent loads according to the balance coordinate system, and the load can be output directly in real time. After the balance output signal is stable, the steel wire is cut immediately to generate a step load. The step-load acquisition device based on SVDC is relatively simple and convenient, and the magnitude, direction, and action point of the single vector are not limited. Also, the SVDC method is no longer dynamic calibration of the balance alone but rather of the whole FMS. This dynamic calibration method is more consistent with an actual shock-tunnel force test.

2.2. Data acquisition of balance signal in time domain

Considering the operating factors of the JF-12 shock tunnel, the same step-load acquisition device based on SVDC was built outside the shock tunnel, comprising the model, the balance, and the supporting structure. As shown in Fig. 2, the model was a standard cone with a length of 0.75 m and a half-cone angle of 10°, the balance was a three-component pulse-type strain-gauge balance, and the three components were the normal force, the pitching moment, and the axial force; the model and balance were supported by a cantilever sting. The Data Acquisition System (DAS) of balance signal comprised a NI PXIe-1071 high-performance acquisition device, a NI PXIe-8880 controller, and a NI PXIe-4330 eight-channel capture card with a maximum sampling rate of 102.4 kS/s and 24-bit resolution. The dynamic sample data acquisition and processing software was developed based on the LabView Professional Development System and was capable of high-precision multi-component dynamic signal acquisition.

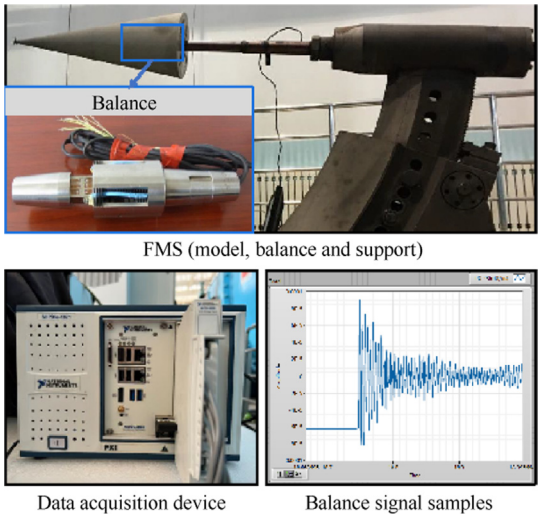

Fig. 2 Force Measurement System (FMS) and Data Acquisition System (DAS) of balance signal.

In this paper, dynamic calibration of the whole FMS was conducted based on SVDC technology, and the implementation steps are shown in detail as follows:[39]

(1) The same FMS in Fig. 2 is built, which is assembled by the model, the three-component pulse-type strain-gauge balance, and the sting supporting structure.
(2) The DAS is connected to the balance output of the FMS, and the balance signal can be recorded in real time.
(3) Without loading, the zero-load output of the balance is recorded by the DAS and used as the benchmark data.
(4) The steel wire is suspended at the head point on the windward surface of the model. At this time, the signals which contain three-component step loads output by the FMS are recorded.
(5) Cut the steel wire when the FMS and DAS are stable. The signals recorded by the DAS are decomposed automatically, and the value, the direction and the point of the step loads are recorded.

We collected 120 groups of the balance signal sample, and each sample comprised two groups of data: the balance step signal and the ideal step signal (corresponding to the input and target data, respectively, in the intelligent model). We selected a sample and plotted its waveform in the time domain, as shown in Fig. 3, where the red line corresponds to the balance step signal (used to simulate the impact generated by the shock-tunnel flow field) and the blue line corresponds to the ideal step signal (used to simulate the simplified aerodynamic force signal). The sampling rate was 50 kHz and the total time for a sample was 150 ms, so the number of points per sample was 7500. The signal was divided into two sections by the starting moment of the flow field during the force test; the zero sig-

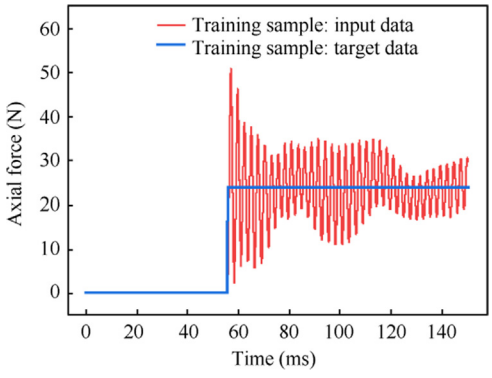

Fig. 3 Balance sample waveform in time domain (axial force).

nal before the step corresponds to the preparation duration before the flow field started. At approximately 55 ms, the signal has a step change, and the edge trigger time can be ignored. Subsequently, the balance step signal contains both aerodynamic force and inertial vibration, whereas the ideal step signal contains no vibration signal and remains stable.

2.3. Time-frequency conversion of balance signal samples

The balance output signal collected during a force test is a typical unsteady and multifrequency impulse signal, and its waveform in the time domain reflects the aerodynamic trend directly. The frequency distribution of the signal can be displayed in the spectrum diagram in the frequency domain, and the vibration interference component can be distinguished by analyzing that diagram.

As a common signal processing method, a Fourier transform can decompose a signal linearly from the time domain into the frequency domain via the triangular basis function; similarly, an inverse Fourier transform can map a signal linearly from the frequency domain into the time domain. The respective transformation equations are

$$F(\omega) = \mathscr{F}[f(t)] = \int_{-\infty}^{+\infty} f(t)\mathrm{e}^{-\mathrm{i}\omega t}\mathrm{d}t \tag{1}$$

$$f(t) = \mathscr{F}^{-1}[F(\omega)] = \frac{1}{2\pi}\int_{-\infty}^{+\infty} F(\omega)\mathrm{e}^{\mathrm{i}\omega t}\mathrm{d}\omega \tag{2}$$

where ω is frequency, $F(\omega)$ is the image function of $f(t)$, and $f(t)$ is the primitive function of $F(\omega)$. There is an inverse relationship between signal resolution in the time domain and that in the frequency domain: the product of the impulse width in the time domain and the bandwidth in the frequency domain is constant, i.e., the narrower the signal pulse in the time domain, the wider the main band in the frequency domain.

A Fast Fourier Transform (FFT) is used to convert the time-domain signal in Fig. 3 into the frequency domain, and its spectrum diagram is shown in Fig. 4. As can be seen, the main frequency of the balance step signal is approximately 380 Hz, whereas this frequency is absent from the ideal step signal, thereby indicating that the inertial vibration frequency of the FMS is approximately 380 Hz.

Because the time-domain signal offers a more direct reflection of the force trend, after analyzing the frequency-domain signal, the latter is transformed into the time domain using an Inverse FFT (IFFT). There may be some loss in the time–frequency conversion, but comparing the original balance signal with the signal after time–frequency conversion as shown in Fig. 5, we can see that they basically coincide completely. This indicates that the loss in time–frequency conversion can be ignored completely, thereby providing a theoretical basis for the feasibility and reliability of data processing in the frequency domain.

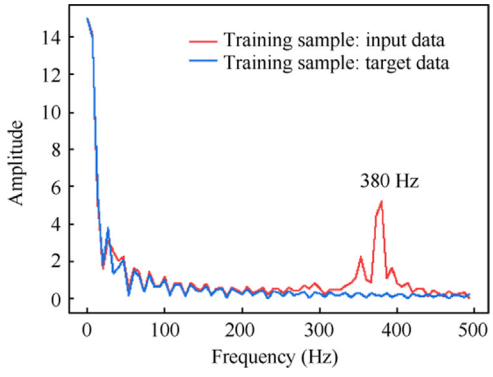

Fig. 4 Balance sample spectrum diagram in frequency domain.

Therefore, the aim in this paper is to take the balance step signal as the input data and the ideal step signal as the target data and build an RNN time-domain model and a CNN frequency-domain model to learn the interference features; the intelligent models can identify and eliminate the interference signal and output a "pure" aerodynamic signal. The trained models are then applied to a shock-tunnel force test to obtain aerodynamic signals without initial interference, thereby ensuring the accuracy of the force measurement results.

3. Dynamic calibration based on RNN time-domain model

3.1. Construction of RNN time-domain model

Feature extraction is a very important but difficult task for a complex artificial-intelligence problem. Deep learning approximates complex functions by stacking multilayer nonlinear mappings, automatically learns hierarchical feature representations from the original data, and uses these combined features to solve complex problems.[40,41] Aimed at the vibration interference signal in the balance signal samples, the neural-network model is built based on supervised learning in deep learning; the intelligent model can automatically extract the basic features of the vibration interference signal and combine them into more-complex features so as to identify the vibration interference signal.

As a common type of neural network in deep learning, RNNs are used mainly to solve time-series problems and predict sequential data. The RNN model has the function of "memory" and the nodes between each two layers are connected.[42] As shown in Fig. 6, the input of the hidden layer comprises the output of the input layer and the hidden layer at the previous moment. For the current moment t, the hidden unit h_t accepts the current input-layer data x_t and the previous hidden-layer data h_{t-1} to generate the output-layer data o_t. Because of the existence of a retarder, the recurrent hidden layer completes the storage and dependence by providing a path for information transmission. Therefore, an RNN can process time-sequence data effectively.

In the process of model training, a sample sequence that is too long will lead to gradient disappearance and gradient explosion during optimization. To solve this problem, Long Short-Term Memory (LSTM) was proposed.[43] LSTM adds a "gate" structure to the RNN unit and selectively affects the state of each moment in the RNN through such structures. It has been shown that the RNN model with the LSTM structure outperforms the standard RNN model. Meanwhile, in the standard RNN model, the state transmission of each layer is one way from front to back, but in practice the output at the current moment is related to that at the previous moment and the later state. Therefore, it is necessary to use a Bidirectional RNN with LSTM (Bi-LSTM), the structure of which is shown in Fig. 7.

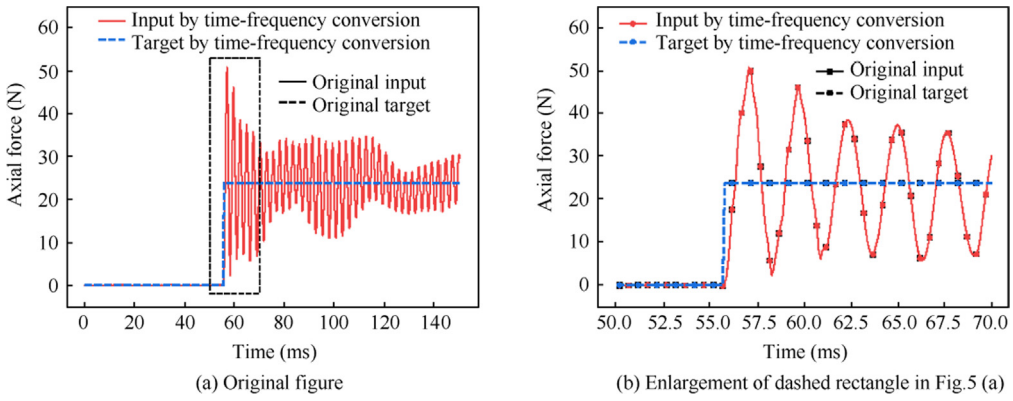

Fig. 5 Verification of signal after time-frequency conversion.

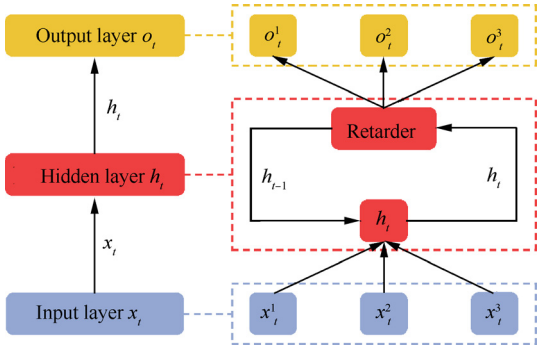

Fig. 6 Unit of a Recurrent Neural Network (RNN).

After collecting the balance signal samples, they are shuffled randomly and divided into several batches. When training the RNN time-domain model, 80 % of the samples are used to train the model and learn the network parameters, while the other 20 % of the samples are used for validation in verification calibration tests.

To ensure consistent training samples and shock-tunnel force measurement data (test samples), the balance output signal is normalized before model training, and the data are mapped to a small specific interval. This data normalization facilitates the model training and improves the model convergence speed and calculation accuracy. After the training, to verify the calculation results more conveniently, the data are inverse-normalized. When normalizing the data, the balance output signal value is mapped to [−1,1] using the linear function:

$$x^* = \frac{x}{\max(|x|)} \tag{3}$$

where x corresponds to the original data, $\max(|x|)$ is the largest absolute value in the original data, and x^* corresponds to the normalized data. After the training, the inverse-normalization function

$$x = \max(|x|)x^* \tag{4}$$

is used to restore the data to the original interval.

The RNN time-domain model was constructed based on Bi-LSTM. The number of the training samples is 120 and the number of the points per training sample is 7500. The output channels of the three-component balance are the normal force, the pitching moment, and the axial force. Therefore, the shapes of the input and output layer of the RNN time-domain model are $(120, 7500, 3)$. After comparing the results of different hidden layers, we confirm that the number of the hidden layers is 3 and the layer parameters are shown in Table 1.

3.2. Validation and error analysis of RNN time-domain model results

As shown in Fig. 8, we select a representative validation sample and compare it with its output data processed by the RNN time-domain model of axial force; the red and black lines represent the input and target data, respectively, and the blue line represents the output signal processed by the RNN time-domain model. Fig. 8 shows that most of the vibration signals in the input data have been eliminated; the blue line almost coincides with the black line, meaning that the output signal

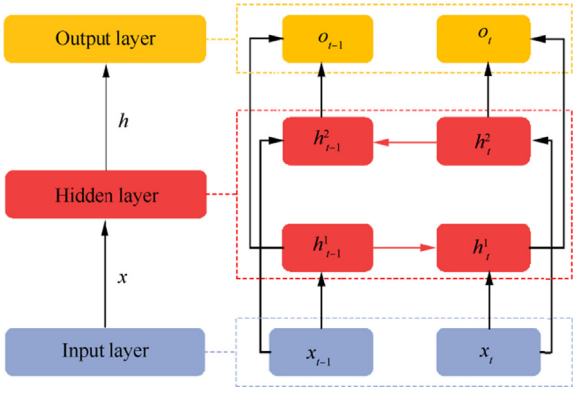

Fig. 7 Unit of a Bidirectional RNN with Long Short-Term Memory (Bi-LSTM).

Table 1 Layer parameters of RNN time-domain model.

Layer	Type	Output shape
Input_1	Input	(120, 7500, 3)
Bi-LSTM_2	Bidirectional LSTM	(120, 7500, 128)
Bi-LSTM_3	Bidirectional LSTM	(120, 7500, 128)
Bi-LSTM_4	Bidirectional LSTM	(120, 7500, 128)
Output_5	Output	(120, 7500, 3)

meets the requirements of the ideal step signal. The value of the processed data is approximately 0 before the signal step and remains constant thereafter, so the signal processed by the RNN time-domain model achieves a steady state and most of the vibration interference signals are eliminated.

The normal force and pitching moment are processed in the same way, and their comparison results are shown in Fig. 9. As can be seen, the processed results of the RNN time-domain model are relatively good and achieve the expected effect.

Herein, we use the Mean Squared Error (MSE) as a loss function to evaluate the data processing capability of the intelligent models: the smaller the MSE, the better the quality of the predicted test data. Fig. 10 shows how the loss of the RNN time-domain model changes with the training time (epoch), where the red and blue lines represent the training and validation losses, respectively, in the model training process. The model loss is approximately 10^{-2} initially, and with more epochs it decreases gradually and becomes steady. After 20000 epochs, the model validation loss has decreased to 3×10^{-5}, which is deemed sufficiently small and basically steady. This indicates that the model has converged and reached the standard for effective dynamic calibration, thereby verifying the feasibility of the data processing method of the RNN time-domain model.

To evaluate more intuitively the quality of the data processed by the RNN time-domain model, we use the relative error δ and the relative standard deviation RSD to evaluate the accuracy and precision of the model. These are calculated as

$$\delta = \frac{\bar{F}^* - \bar{F}}{\bar{F}} \times 100\% \tag{5}$$

$$\mathrm{RSD} = \frac{1}{\bar{F}^*}\sqrt{\frac{1}{N-1}\sum_{i=1}^{N}\left(F_i^* - \bar{F}^*\right)^2} \times 100\% \tag{6}$$

We analyze the step signals in Figs. 8 and 9, i.e., the data in the interval of 60–140 ms. Here, $\bar{F}$ is the mean value of the ideal step signal (used to represent the "true" force) and $\bar{F}^*$ is the mean value of the results processed by the RNN time-domain model (used to represent the approximate force).

The calculation results are given in Table 2. As can be seen, the relative errors of the RNN time-domain model are relatively small, especially that for the axial force, which is less than 0.1%, indicating that the accuracy of the model is relatively high. Meanwhile, the relative standard deviations of the three components are also relatively small, being basically less than 1%, indicating the high precision of the model. The model achieves high accuracy in the overall data processing, with that of the axial force being obviously better than those of the normal force and pitching moment. One reason for this is that while acquiring balance samples, the inertial vibration characteristic of the axial force component is more obvious and its signal periodicity is stronger, whereas the other two components suffer greatly from environmental noise; another reason is that the accuracy of static calibration for the axial force is better than those for the normal force and pitching moment. Therefore, the subsequent analysis is focused on the axial force and not the other two components.

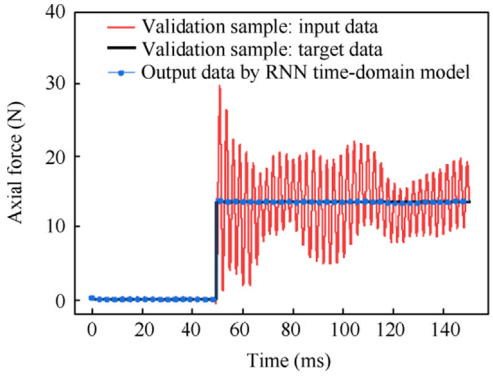

Fig. 8 Validation of axial force processed by RNN time-domain model.

4. Dynamic calibration based on CNN frequency-domain model

4.1. Construction and optimization of CNN frequency-domain model

When a force measurement is conducted in a shock tunnel, the balance output signal is rather complex, containing the aerodynamic force, inertial vibration, and other interference signals. The aerodynamic force and inertial vibration of the FMS differ greatly in the frequency domain: the aerodynamic signal is affected by the shock-tunnel flow field and other factors, so its frequency varies with time, whereas the inertial vibration fre-

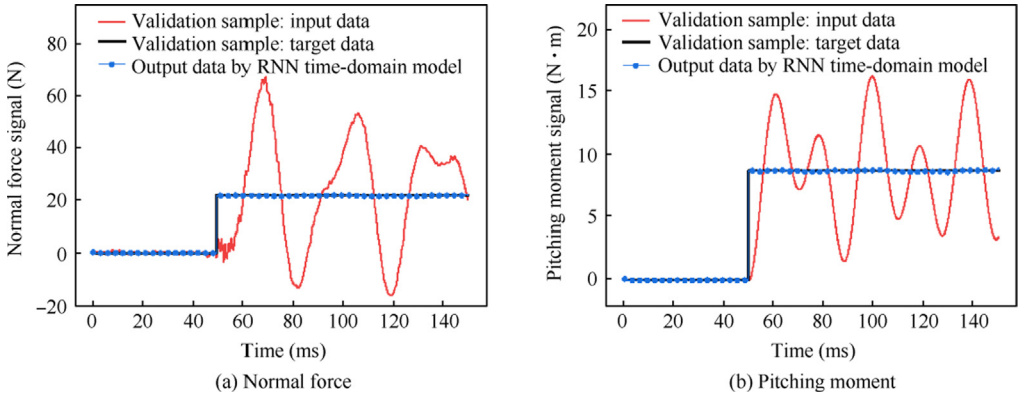

Fig. 9 Validation of processing by RNN time-domain model.

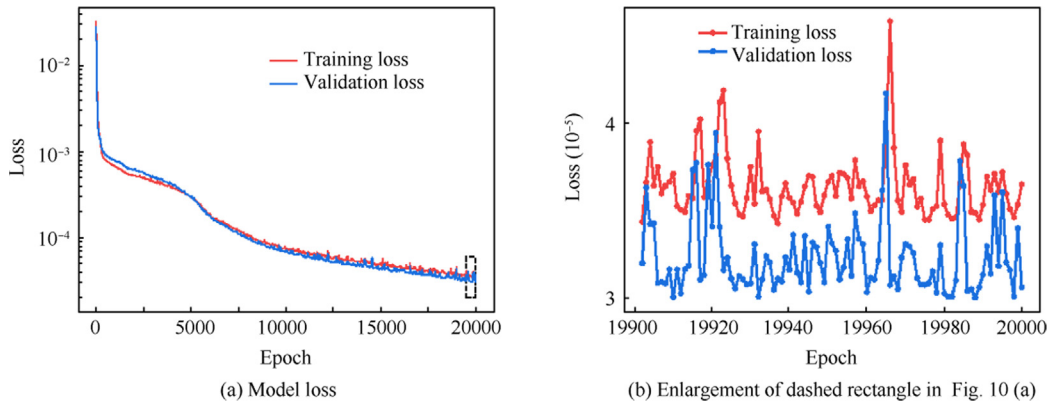

Fig. 10 Loss of RNN time-domain model decreases with number of epoch.

Table 2 Relative error and relative standard deviation of RNN time-domain model.

Component	$\bar{F}$	$\bar{F}^*$	δ(%)	RSD (%)
Normal force	21.955 N	21.632 N	−1.47	0.582
Pitching moment	8.694 N·m	8.674 N·m	−0.229	0.561
Axial force	13.489 N	13.482 N	−0.0506	0.433

quency is an inherent attribute of the system; when the mass and structure of the FMS are determined, the inertial vibration frequency is also determined and remains stable within the test duration. Therefore, the frequency-domain signal reflects the inertial vibration characteristics of the FMS more accurately in essence.

As a classic neural network in deep learning, a CNN embodies convolutional calculations and a depth structure. Because of its local connections, shared weights, and pooling layer, a CNN's complexity and training parameters are greatly reduced, while its computing capability is very strong. CNN models have been used widely in image recognition, sentence classification, data fitting, and other intelligent fields.[44] The recognition of the inertial vibration feature of the FMS in the frequency domain tends to be an image recognition problem, so we use a CNN to build a frequency-domain model for recognizing the inertial vibration feature.

A CNN model generally contains an input layer, some hidden layers, and an output layer, of which the hidden layers include convolutional, pooling, and fully connected layers. In the model training process, the loss decreases with more epochs, and the model converges finally through minimizing the loss. Fig. 11 shows a flowchart of the CNN frequency-domain model. The input and output layer comprise the balance signal samples processed by FFT and the expected results processed by the model, respectively. The model is constructed based on several two-dimensional convolutional neural networks, because the data processed by FFT in input layer is complex, including the real and imaginary components. Therefore, the shapes of the input and output layer of the model are $(120, 2, 7500, 3)$. The hidden layers comprise several convolutional and pooling layers. The number and size of the convolutional kernel in a convolutional layer affect the model results to a great extent, and the pooling layer accelerates the calculations and prevents overfitting.

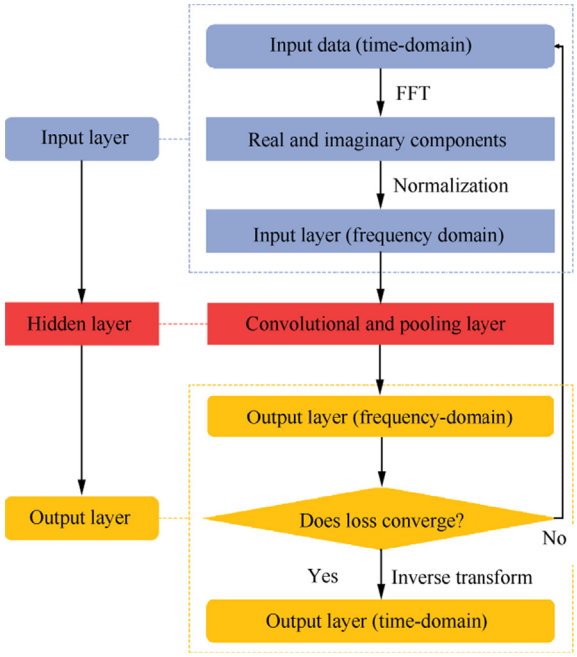

Fig. 11 Flowchart of a Convolutional Neural Network (CNN) frequency-domain model.

In deep learning, the training accuracy and time are usually used to evaluate the quality of a neural-network model. The quality of a CNN model is improved mainly by adjusting the training and structure parameters: the training parameters are generally the specific parameters of the training process, including the learning rate and number of epochs, while the structure parameters are mainly some parameters in the hidden layer, including the number of convolutional layers and the

number and size of the convolutional kernel in each convolutional layer. The structural and training parameters have a decisive impact on the quality and training time of the model. However, limited by the principle of the method, there is no theoretical basis for how to select the parameters, so it depends on experience. In general, we set several groups of candidate values, and then choose the best value through test. To optimize the model quality, we determine the initial training parameters, then change the structure parameters gradually, and finally adjust the training parameters to optimize the model. Considering the computational cost, the number of convolutional layers and epochs are adjusted to improve the model results. According to the experience, we set the initial number of convolutional layers to 64, the initial epochs to 50000, and the initial learning rate to 10^{-5}.

The number of convolutional layers can directly affect the training time and accuracy of the model. Increasing the number of convolutional layers can reduce the number of parameters when the model achieves the same expressiveness. Keeping the other parameters the same, we calculate the relative error and relative standard deviation with different numbers of convolutional layers based on Eqs. (5) and (6). The comparison results when the number of convolutional layers is 24, 64 and 96 are shown in Table 3.

According to Table 3, when the number of convolutional layers increases from 24 to 96, it can be found that the relative error increases gradually, while the relative standard deviation decreases obviously, and the training time increases obviously. Therefore, considering them comprehensively, the number of convolutional layers is determined to be 64.

After determining the number of convolutional layers, the number of epochs is optimized. Increasing the number of epochs can improve the accuracy of the model, but the training time will increase significantly. The relative error and relative standard deviation with different numbers of epochs are shown in Table 4.

Table 4 shows the results processed by the CNN frequency-domain model when the number of epochs is 10000, 50000 and 100000 respectively. It can be seen that when the number of epochs increases, the relative error increases, and the relative standard deviation decreases. Therefore, we choose the number of epochs as 100000.

After the above comparison, the parameters of the CNN frequency-domain model are optimized, and the finally number of convolutional layers and epochs are 64 and 100000, respectively.

4.2. Validation and error analysis of results from CNN frequency-domain model

The optimized CNN frequency-domain model is used to process the dynamic samples. To analyze the model quality more intuitively, the output signal processed by the model is compared with the ideal step signal in the frequency and time domains as shown in Fig. 12, where the blue line represents the output signal processed by the model. As can be seen, in the frequency domain, the inertial vibration interference of 380 Hz in the input data is eliminated completely, and in the time domain, the output signal obviously meets the requirement of the ideal step signal.

Table 3 Comparison with different numbers of convolutional layers of CNN frequency-domain model.

Convolutional layer number	$\bar{F}$(N)	$\bar{F}^*$(N)	δ(%)	RSD (%)
24	12.745	12.735	−0.08	0.94
64	12.745	12.530	−1.69	0.39
96	12.745	12.475	−2.12	0.29

Table 4 Comparison with different numbers of epochs of CNN frequency-domain model.

Epoch number	$\bar{F}$(N)	$\bar{F}^*$(N)	δ(%)	RSD (%)
10000	12.745	12.720	−0.20	2.19
50000	12.745	12.580	−1.29	1.00
100000	12.745	12.530	−1.69	0.39

Similar to those with the RNN time-domain model, we calculate the relative error and relative standard deviation of the CNN frequency-domain model, as given in Table 5. The mean of the output data processed by the model is close to that of the ideal step signal, and its relative error is approximately 2%, which verifies that the accuracy is high and the model is reliable. Also, the relative standard deviation is only 0.39%, indicating that the output data are very steady during this period. Therefore, the CNN frequency-domain model has high accuracy and precision and is very reliable for data processing.

5. Intelligent data processing of force measurements from JF-12 shock tunnel

The validation and analysis of the RNN time-domain and CNN frequency-domain models show that they dealt very well with the inertial vibration interference signals in the training samples, so now we apply these two classic models to dynamic calibration of the FMS in a shock tunnel. In order to verify the reliability of the modeling method, a force measurement experiment was carried out in JF-12 shock tunnel. The experimental model is a standard cone, with a half-cone angle of 10° and a length of 0.75 m (HSCM-2).[45] Fig. 13 shows the force measurement experiment in JF-12 shock tunnel.

After the force measurement experiment, the output signals of balance were reprocessed by the RNN time-domain and CNN frequency-domain models, and the results are shown in Fig. 14. As can be seen, the inertial vibration of 380 Hz is eliminated in the frequency domain, and the output signal processed by the models is mostly free of vibration interference. Compared with the time waveform processed by the RNN time-domain model, that processed by the CNN frequency-domain model is steadier. The results for the validation sample in Fig. 12 are better than those for the test sample in Fig. 14, the main reason being that the test signal is more complex and the real aerodynamic signal is not absolutely steady; there is still a certain amount of deviation between the processed signal and the ideal step signal.

Similar to the data processing method for the training samples, we calculate the relative deviation (RD) and the relative standard deviation (RSD) for the RNN time-domain and CNN frequency-domain models. The results in Table 6 show

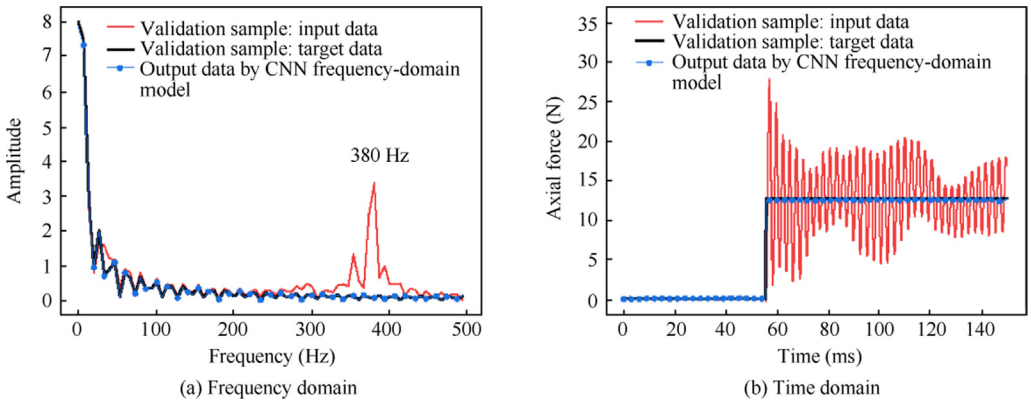

Fig. 12 Validation of axial force processed by CNN frequency-domain model.

Table 5 Relative error and relative standard deviation of CNN frequency-domain model.

Component	$\bar{F}$(N)	$\bar{F}^*$(N)	δ(%)	RSD (%)
Axial force	12.745	12.530	−1.69	0.39

Fig. 13 Force test in JF-12 shock tunnel.

that after the force measurement signal is processed by these two intelligent models, the relative error is sufficiently small, indicating that the current method has high accuracy in processing the shock-tunnel balance signal and can recognize the inertial vibration features of the FMS effectively. Deep-learning modeling based on an RNN in the time domain and a CNN in the frequency domain has high application value in processing dynamic force measurement signals from shock tunnels, and we will continue to carry out more in-depth research on the cross-application of deep-learning technology in dynamic signal analysis. The next step in model training will be to increase the numerical number of samples. Meanwhile, in the process of sample acquisition, the environmental noise can be eliminated properly to ensure consistency between training and test samples to improve the model quality.

Table 6 Comparison of RNN time-domain and CNN frequency-domain models (axial component).

Model	$\bar{A}$	$\bar{A}^*$	RD (%)	RSD(%)
RNN	0.1026	0.1031	0.49	16.49
CNN	0.1026	0.1012	−1.36	6.56

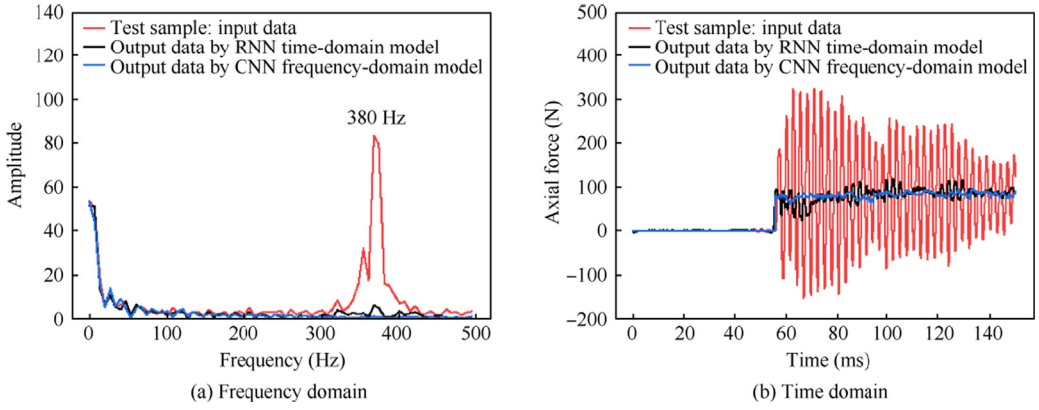

Fig. 14 Comparison of axial force processed by RNN time-domain and CNN frequency-domain models.

The results contain some uncertainties due to the systematic and random errors in determining the freestream properties and calibrating the balance, among other sources. According to the numerical calculation method, the uncertainties can be defined as Types A and B standard uncertainty, where the Type A uncertainty of the modeling method is mainly from the combined loading repeatability and error, while the Type B uncertainty is mainly from the load source, the data acquisition system, and the calibration equipment.[46] The uncertainty u_{i1} and u_{i2} introduced by the combined loading repeatability and error can be calculated by Eqs. (7) and (8), respectively.

$$u_{i1} = \frac{1}{X_{\max,i}\sqrt{n(n-1)}}\sqrt{\sum_{j=1}^{n}\left(X_{ij} - \frac{1}{n}\sum_{j=1}^{n}X_{ij}\right)^2} \times 100\%\ i = 1,2,3;\ j = 1,2,...,n \tag{7}$$

where X and $X_{\max,i}$ represent the load output by the balance and the maximum design load, n represents the number of repeated loads, and the subscript i and j represent the i component and the j repeated load, respectively.

$$u_{i2} = \frac{1}{X_{\max,i}\sqrt{n-1}}\sqrt{\sum_{j=1}^{n}\left(F_{ij} - P_{ij}\right)^2} \times 100\%\ i = 1,2,3;\ j = 1,2,...,n \tag{8}$$

where F and P represent the processed load by the modeling method and real load output by the balance, respectively.

To obtain more accurate results, we perform a preliminary analysis of their uncertainty, and through post-processing, a conservative assessment is that the expanded uncertainty of axial force is about $\pm 5.0\% \sim$ FS (95% confidence interval). Therefore, the accuracy of the FMS based on deep learning has been further verified.

6. Conclusions

(1) According to different characteristics of the balance signal in the time domain and the frequency domain, the corresponding intelligent models were proposed. An RNN model in the time domain and a CNN model in the frequency domain were trained to process the balance signal, and the results show that the two intelligent models recognized the inertial vibration characteristics of the FMS effectively.

(2) The aerodynamic signals processed by the models were steady and the relative error of each component was about 1%. The reliability of this modeling method was verified by comparing the results processed by the models with international standard.

(3) The proposed modeling method is universal in force tests in shock tunnel. The RNN model and CNN model can be used to process the complex characteristics in the time domain and the frequency domain, respectively. The present modeling method based on deep learning is feasible for shock-tunnel force tests and has great engineering value. Exploring new data processing techniques with different neural-network models could provide more reliable data for research in hypersonic vehicles.

Declaration of Competing Interest

The authors declare that they have no known competing financial interests or personal relationships that could have appeared to influence the work reported in this paper.

Acknowledgements

This work was supported by the National Natural Science Foundation of China (Nos. 11672357, 11727901).

References

1. Baals DD. Wind tunnels of NASA. Washington, D.C.: NASA; 1981.
2. Squire LC. A review of the role of some small high-speed wind tunnels in aeronautical research. *Prog Aerosp Sci* 1998;**34**(3–4):107–66.
3. Zong Q, Zeng FL, Zhang XB, et al. Modeling and model verification of hypersonic aircraft. Beijing: Science Press; 2016 [Chinese].
4. He DX. Wind tunnel balance. Beijing: National Defence Industry Press; 2001 [Chinese].
5. Bernstein L, Pankhurst RC. Force measurements in short-duration hypersonic facilities. Pairs: Advisory Group For Aerospace Research and Development Neuilly-Sur-Seine; 1975.
6. Naumann KW, Ende H, Mathieu G. Technique for aerodynamic force measurement within milliseconds in shock tunnel. *Shock Waves* 1991;**1**(3):223–32.
7. Storkmann V, Olivier H, Gronig H. Force measurements in hypersonic impulse facilities. *AIAA J* 1998;**36**(3):342–8.
8. Sanderson SR, Simmons JM. Drag balance for hypervelocity impulse facilities. *AIAA J* 1991;**29**(12):2185–91.
9. Mee DJ, Daniel WJT, Simmons JM. Three-component force balance for flows of millisecond duration. *AIAA J* 1996;**34**(3):590–5.
10. Smith AL, Mee DJ, Daniel WJT, et al. Design, modelling and analysis of a six component force balance for hypervelocity wind tunnel testing. *Comput Struct* 2001;**79**(11):1077–88.
11. Robinson MJ, Mee DJ, Tsai CY, et al. Three-component force measurements on a large scramjet in a shock tunnel. *J Spacecr Rockets* 2004;**41**(3):416–25.
12. Robinson MJ, Schramm JM, Hannemann K. Design and implementation of an internal stress wave force balance in a shock tunnel. *CEAS Space J* 2011;**1**(1):45–57.
13. Duryea GR, Martin JF. An improved piezoelectric balance for aerodynamic force. *IEEE Trans Aerosp Electron Syst* 1968;**AES-4**(3):351–9.
14. Li SC, Li KS, Liu BK, et al. A new dynamic modelling methodology of a force measuring system for hypersonic impulse wind tunnel. *Measurement* 2020;**164**:108012.
15. Li SC, You ZC, Gao HL, et al. Force measurement and support integrated device in hypersonic wind tunnel. *IEEE Trans Instrum Meas* 2022;**71**:1–9.
16. Naumann KW, Ende H, Mathieu G, et al. Millisecond aerodynamic force measurement with side-jet model in the ISL shock tunnel. *AIAA J* 1993;**31**(6):1068–74.
17. Laurence SJ, Butler CS, Martinez Schramm J, et al. Force and moment measurements on a free-flying capsule in a shock tunnel. *J Spacecr Rockets* 2018;**55**(2):403–14.
18. Tanno H, Komuro T, Sato K, et al. Free-flight measurement technique in the free-piston high-enthalpy shock tunnel. *Rev Sci Instrum* 2014;**85**(4):045112.

19. Mizuno T, Ishino Y, Takasaki M. Fabrication of a three-dimensional force measurement system using double series magnetic suspension. *IFAC-PapersOnLine* 2016;**49**(21):536–40.
20. Wang YP, Liu YF, Luo CT, et al. Force measurement using strain-gauge balance in a shock tunnel with long test duration. *Rev Sci Instrum* 2016;**87**(5):055108.
21. Wang Y, Liu Y, Jiang Z. Design of a pulse-type strain gauge balance for a long-test-duration hypersonic shock tunnel. *Shock Waves* 2016;**26**(6):835–44.
22. Wang Y, Jiang Z. Impulse force-measurement system. *Shock Waves* 2020;**30**(6):603–13.
23. Sahoo N, Mahapatra DR, Jagadeesh G, et al. An accelerometer balance system for measurement of aerodynamic force coefficients over blunt bodies in a hypersonic shock tunnel. *Meas Sci Technol* 2003;**14**(3):260–72.
24. Joarder R, Jagadeesh G. A new free floating accelerometer balance system for force measurements in shock tunnels. *Shock Waves* 2003;**13**(5):409–12.
25. Tanno H, Komuro T, Takahashi M, et al. Unsteady force measurement technique in shock tubes. *Rev Sci Instrum* 2004;**75**(2):532–6.
26. Saravanan S, Jagadeesh G, Reddy KPJ. Aerodynamic force measurement using 3-component accelerometer force balance system in a hypersonic shock tunnel. *Shock Waves* 2009;**18**(6):425–35.
27. Marineau EC, MacLean M, Mundy EP, et al. Force measurements in hypervelocity flows with an acceleration compensated strain gage balance. *J Spacecr Rockets* 2012;**49**(3):474–82.
28. Lv JZ, Zhang XQ, Chen GX, et al. Transient dynamics research on the force-measurement system for hypersonic impulse combustion wind tunnel based on inertia compensation. *J Aerosp Eng* 2018;**31**(6):04018094.
29. Lv JZ, Zhang X, Chen G, et al. Transient simulation for dynamic output of force measuring balance in an impulse combustion wind tunnel based on inertia compensation. *J Vib Shock* 2018;**37**(2):216–22 [Chinese].
30. Luo CT, Wang YP, Wang C, et al. Wave system fitting: a new method for force measurements in shock tunnels with long test duration. *Mech Syst Signal Process* 2015;**62–63**:296–304.
31. Luo C, Wang Y, Hu Z, et al. Weighting by cross-validation: A calibration method for force measurements via transient response analysis. *Exp Tech* 2019;**43**(4):469–78.
32. Nie SJ, Wang YP. Signal analysis and processiong of shock tunnel balance based on time-frequency transform. *Chinese J Theor Appl Mech* 2022;**54**(1):232–43 [Chinese].
33. Wang YP, Yang RX, Nie SJ, et al. Deep-learning-based intelligent force measurement system using in a shock tunnel. *Chinese J Theor Appl Mech* 2020;**52**(5):1304–13 [Chinese].
34. Wang QC, Li SC, Gao HL, et al. Research on intelligent identification algorithms for short-term aerodynamics of hypersonic wind tunnels. *Chinese J Theor Appl Mech* 2022;**54**(3):688–96 [Chinese].
35. Wang YP, Hu ZM, Liu YF, et al. Starting process in a large-scale shock tunnel. *AIAA J* 2016;**54**(4):1240–9.
36. Garland PP, Rogers RJ. Dynamic calibration of tri-axial piezoelectric force transducers. *Meas Sci Technol* 2008;**19**(9):095202.
37. Li B. Characteristics' experimental study on the 6-ssr six degree-of-freedom accelerometer[dissertation]. Qinhuangdao: Yanshan University; 2011 [Chinese].
38. Yang SL. Studies on dynamic characteristics and dynamic correction methods for wind tunnel strain gauge balance[dissertation]. Hefei: Hefei University of Technology; 2014 [Chinese].
39. Wang YP, Jiang ZL. Intelligent force-measurement system use in shock tunnel. *Sensors (Basel)* 2020;**20**(21):6179.
40. Sun ZJ, Xue L, Xu YM, et al. Overview of deep learning. *Application Res Computers* 2012;**29**(8):2806–10.
41. Du XD, Cai YH, Wang S, et al. Overview of deep learning. *2016 31st Youth Academic Annual Conference of Chinese Association of Automation (YAC)*. Wuhan, China. Piscataway: IEEE; 2017. p. 159–64.
42. De Mulder W, Bethard S, Moens MF. A survey on the application of recurrent neural networks to statistical language modeling. *Comput Speech Lang* 2015;**30**(1):61–98.
43. Van Houdt G, Mosquera C, Nápoles G. A review on the long short-term memory model. *Artif Intell Rev* 2020;**53**(8):5929–55.
44. Yao GL, Lei T, Zhong JD. A review of convolutional-neural-network-based action recognition. *Pattern Recognit Lett* 2019;**118**:14–22.
45. General Armament Department of Chinese People's Liberation Army. Aerodynamic test method in hypersonic wind tunnel. Beijing: General Armament Department of Chinese People's Liberation Army; 2002 [Chinese].
46. General Armament Department of Chinese People's Liberation Army. Specification for wind tunnel strain gage balance. Beijing: General Armament Department of Chinese People's Liberation Army; 2011 [Chinese].